Since January 2020 Elsevier has created a COVID-19 resource centre with free information in English and Mandarin on the novel coronavirus COVID-19. The COVID-19 resource centre is hosted on Elsevier Connect, the company's public news and information website.

Environmental Pollution 286 (2021) 117252

Contents lists available at ScienceDirect

Environmental Pollution

journal homepage: www.elsevier.com/locate/envpol

Haze episodes before and during the COVID-19 shutdown in Tianjin, China: Contribution of fireworks and residential burning☆

Qili Dai [a,b], Jing Ding [b,c], Linlu Hou [a,b], Linxuan Li [a,b], Ziying Cai [c], Baoshuang Liu [a,b], Congbo Song [d], Xiaohui Bi [a,b], Jianhui Wu [a,b], Yufen Zhang [a,b,*], Yinchang Feng [a,b], Philip K. Hopke [e,f]

[a] State Environmental Protection Key Laboratory of Urban Ambient Air Particulate Matter Pollution Prevention and Control, College of Environmental Science and Engineering, Nankai University, Tianjin, 300350, China
[b] CMA-NKU Cooperative Laboratory for Atmospheric Environment-Health Research (CLAER), College of Environmental Science and Engineering, Nankai University, Tianjin, 300350, China
[c] Tianjin Environmental Meteorological Center, Tianjin, 300074, China
[d] School of Geography Earth and Environment Sciences, University of Birmingham, Birmingham, B15 2TT, UK
[e] Department of Public Health Sciences, University of Rochester School of Medicine and Dentistry, Rochester, NY, 14642, USA
[f] Institute for a Sustainable Environment, Clarkson University, Potsdam, NY, 13699, USA

ARTICLE INFO

Keywords:
Haze
COVID-19
$PM_{2.5}$
Air pollution
Sources

ABSTRACT

Potential health benefits from improved ambient air quality during the COVID-19 shutdown have been recently reported and discussed. Despite the shutdown measures being in place, northern China still suffered severe haze episodes (HE) that are not yet fully understood, particularly how the source emissions changed. Thus, the meteorological conditions and source emissions in processing five HEs occurred in Beijing-Tianjin-Hebei area were investigated by analyzing a comprehensive real-time measurement dataset including air quality data, particle physics, optical properties, chemistry, aerosol lidar remote sensing, and meteorology. Three HEs recorded before the shutdown began were related to accumulated primary pollutants and secondary aerosol formation under unfavorable dispersion conditions. The common "business as usual" emissions from local primary sources in this highly polluted area exceeded the wintertime atmospheric diffusive capacity to disperse them. Thus, an intensive haze formed under these adverse meteorological conditions such as in the first HE, with coal combustion to be the predominant source. Positive responses to the shutdown measures were demonstrated by reduced contributions from traffic and dust during the final two HEs that overlapped the Spring and Lantern Festivals, respectively. Local meteorological dispersion during the Spring Festival was the poorest among the five HEs. Increased residential burning plus fireworks emissions contributed to the elevated $PM_{2.5}$ with the potential of enhancing the HEs. Our results highlight that reductions from shutdown measures alone do not prevent the occurrence of HEs. To further reduce air pollution and thus improve public health, abatement strategies with an emphasis on residential burning are needed.

1. Introduction

To tackle the serious air pollution issues and protect public health in China, the State Council of China enacted a five-year Air Pollution Prevention and Control Action Plan (also called "Clear Air Action") in 2013 and a three-year action plan to continue fighting air pollution ("Blue Sky Protection Campaign") from 2018 to 2020. The air quality in China has improved since these stringent control measures were implemented (Geng et al., 2019; Vu et al., 2019; Wang et al., 2019; Zhang et al., 2019). The national population-weighed annual mean $PM_{2.5}$ concentrations decreased from 67.4 μg m^{-3} in 2013 to 45.5 μg m^{-3} in 2017 (Xue et al., 2019). However, severe particulate haze episodes (HEs) still periodically occur during the cold season in the North China Plain (NCP), specifically in the Beijing-Tianjin-Hebei region

☆ This paper has been recommended for acceptance by Da Chen.

* Corresponding author. State Environmental Protection Key Laboratory of Urban Ambient Air Particulate Matter Pollution Prevention and Control, College of Environmental Science and Engineering, Nankai University, Tianjin, 300350, China.
E-mail address: zhafox@nankai.edu.cn (Y. Zhang).

https://doi.org/10.1016/j.envpol.2021.117252
Received 10 December 2020; Received in revised form 21 April 2021; Accepted 23 April 2021
Available online 6 May 2021

(BTH) and its surroundings. According to the "Technical Regulation on Ambient Air Quality Index (AQI)" issued by the Ministry of Ecology and Environment of China in 2012 (HJ 633–2012), a high air pollution day is defined as daily AQI greater than 150, which corresponds to daily $PM_{2.5}$ concentrations greater than 150 μg m^{-3}. There were 20 heavy polluted days in 2019 (AQI>200) in the BTH and its surroundings (http://www.mee.gov.cn/hjzl/sthjzk/zghjzkgb/). This region is one of the most severely polluted hotspots in the world because of its high population density with sources including traffic, and many polluting emission sources (Chang et al., 2018, 2019; Wang et al., 2014a, 2014b, 2014c) as well as adjacent periurban areas that continue to use solid fueled stoves for heating and cooking (Zhang et al., 2017).

In December 2019, an outbreak of a novel coronavirus infectious disease (COVID-19) was first identified in Wuhan (Zhu et al., 2020), and rapidly expanded across China. Despite the significant reductions in economic activities and traffic flow after the shutdown began, the NCP region repeatedly suffered severe HEs, so-called "pandemic haze" that attracted much attention from the public to the effectiveness of current mitigation strategies to reduce air pollution (Lv et al., 2020). There are several reports of studies that analyzed the formation mechanisms of these HEs through field measurement data and air quality models (Chang et al., 2020; Huang et al., 2020; Le et al., 2020). Le et al. (2020) concluded that the remaining uninterrupted emissions from power plants and petrochemical facilities coupled with anomalously high air humidity promoted aerosol heterogeneous chemistry. These particulate precursor inputs into the atmosphere along with stagnant airflow and increased atmospheric oxidizing capacity contributed to the unexpected severe haze episodes in northern China. Huang et al. (2020) reported that the atmospheric oxidizing capacity increased because of the reductions in transportation-related NO_x emissions that resulted in increased ozone and nighttime NO_3 radical formation. The resulting secondary aerosol formation offset the reductions in primary emissions. Chang et al. (2020) argued that the synergistic effects of atmospheric chemistry and long-range transport promoting the formation of nitrate were the key elements of the haze formation during the Spring Festival in Shanghai. The COVID-19 shutdown period coincided with the Spring and Lantern Festivals. As the most important festival in China, people normally ignite fireworks to celebrate the festival (Lai and Brimblecombe, 2020; Pang et al., 2021; Tian et al., 2014). In addition to fireworks displays, "Sheng Wang Huo" (making a fire) is another long history tradition that sets off celebratory bonfires in northern China, particularly in Shanxi, Hebei, and Inner Mongolia provinces (https://www.chinadaily.com.cn/m/shanxi/datong/2011-09/28/content_13813263.htm). Although such activites were gradually banned in urban areas by local governments in recent years, it remains unclear how the festival-related emissions contributed to the haze episodes during this period with significant reductions in shutdown-associated emission sources.

A clear definition of a haze episode is necessary before further analysis. Based on the annual grade-II limit values set by the National Ambient Air Quality Standards of China (GB3095-2012), Wang et al. (2014c) defined haze episodes as two successive days with daily $PM_{2.5}$ concentrations greater than 75 μg m^{-3}. Zheng et al. (2016) modified this definition by replacing the daily $PM_{2.5}$ concentration by the 24 h moving average $PM_{2.5}$ concentration and adding an additional criterion, an hourly concentration threshold of 35 μg m^{-3} (equals to the NAAQS grade I standard), to separate polluted/clean hours and thereby capture the pollution duration. To focus exclusively on very high pollution events, we slightly modified the two elements in the haze definition from Zheng et al. (2016) (Fig. S1): The 24 h moving average $PM_{2.5}$ concentration increased from 75 to 150 μg m^{-3} and the hourly concentration threshold of 35 μg m^{-3} was set at 75 μg m^{-3}. An in situ real-time comprehensive observation dataset from a measurement campaign from January 1 to February 15, 2020, including five high HEs recorded before and during the COVID-19 shutdown, was investigated in this work. To examine the impact of meteorology and emissions in processing these HEs, tracer gas pollutants, $PM_{2.5}$ compositions, particle number concentrations, ground-based aerosol lidar remote sensing, and a series of meteorological parameters derived from tower-based observations and wind profiler radar in Tianjin, and the routine air quality data of the five surrounding cities in the BTH area were analyzed. We specifically examined changes in source contributions during the five HEs, which provided additional understanding of the haze formations during this unique shutdown period.

2. Materials and methods

2.1. Data collection

2.1.1. Air pollutants and $PM_{2.5}$ composition

Hourly concentrations of $PM_{2.5}$, PM_{10}, sulfur dioxide (SO_2), nitrogen oxides (NO_2), carbon monoxide (CO) and ozone (O_3) measured in Beijing, Tianjin, Langfang, Tangshan, Cangzhou, and Baoding from January 1 to February 15, 2020 were downloaded from the China National Environmental Monitoring Center (http://106.37.208.233:20035/). In addition, data were obtained from online instruments providing particle chemical species, particle number concentrations along with aerosol lidar and surface meteorological parameters deployed in the Nankai University air quality supersite (38°59′ N, 117°20′ E) (Fig. S2) in the Jinan district of Tianjin, China. The site is ~25 km southeast of downtown Tianjin, representing a typical suburban area and away from major highways. Chemical species of $PM_{2.5}$ were measured with an in situ X-ray fluorescence instrument (Focused Photonics Inc., China) for elements (Al, Si, Ca, Ti, V, Cr, Mn, Fe, Ni, Cu, Zn, As, Ba, and Pb), an in situ ion chromatograph (Thermo Fisher Scientific Inc., USA) for water-soluble ions (SO_4^{2-}, NO_3^-, NH_4^+, Cl^-, K^+, Mg^{2+}, and Ca^{2+}), and a semi-continuous thermal-optical carbon analyzer (Focused Photonics Inc., China) for organic carbon (OC) and element carbon (EC). Instrument calibrations and sampling fiter replacement were performed regularly. All instruments were remotely monitored and checked on-site to avoid misfunction. All instruments were equipped with a $PM_{2.5}$ inlet. The detailed instrumentation information and maintenance as well as quality assurances and control are available in Tian et al. (2020) and Dai et al. (2020a,b).

2.1.2. Meteorological data

Meteorological parameters include air temperature (T), relative humidity (RH), wind direction (WD) and wind speed (WS) were recorded at heights of 5, 10, 20, 30, 40, 60, 80, 100, 120, 140, 160, 180, 200, 220, and 250 m AGL from a meteorological tower (39°04′N, 117°12′E) suited in downtown of Tianjin. Vertical wind profiles in both the horizontal and vertical directions were measured with a wind profile radar in rural Tianjin (39°04′N, 117°03′E). Solar radiation was measured with a sun photometer (Kipp & Zonen Inc., Netherlands) in the supersite. Measurements from an aerosol lidar (CAS Photonics Co., Ltd., China) deployed in the supersite were also collected, which is capable of identifying the regional transport in the upper atmosphere (>200 m AGL). The near-surface transport cannot be inferred from aerosol lidar here. Mixing layer height (MLH) was recorded using a ceilometer (Vaisala Inc., Finland) at the Tianjin Eco-Environmental Monitoring Station (39°06′N, 117°09′E).

2.2. Source apportionment

Source contributions to $PM_{2.5}$ were estimated using dispersion normalized positive matrix factorization (DN-PMF) recently presented by Dai et al. (2020). Briefly, the ventilation coefficient (VC) (Tiwari et al., 2016), a measure of atmospheric dilution, was incorporated into PMF analysis, to reduce the dilution effects on source estimates. Six sources include mixed coal combustion, traffic emissions, secondary inorganic aerosol (SIA), soil (+aged sea salt), municipal waste incinerator, and fireworks and residential burning were resolved form DN-PMF.

Residential burning refers to solid fuel (coal or biomass) in commonly used household stoves, for the purpose of providing energy for residential heating and cooking. While coal combustion refers to the use of coal in industrial operations and district heating, with coal burned in boilers at relatively high temperature. Among the six sources, the fireworks and residential burning only appeared after the Spring Festival began, and the residential burning source was unable to be seperately resolved. There should be residential solid fuel burning in the cold period. It would mix with other sources. The coal combustion source was therefore very likely a mixed source, including coal combustion in boilers and also coal burned in residential stoves. Details of the source apportionment of $PM_{2.5}$ during the measurement period are available in Dai et al. (2020).

3. Results and discussion

3.1. Statistics of the haze episodes

The start time of each HE period was set as the time when the hourly $PM_{2.5}$ concentrations first exceeded 75 μg m^{-3}, while the end time was set as the hour prior to the hour in which the $PM_{2.5}$ concentration fell below 75 μg m^{-3}. The duration of each HE was calculated as the difference between the end time and start time. The revised definition of the haze episode is given in Text S1 with a schematic diagram presented in Fig. S1.

The time series of the routine air quality data for Beijing, Tianjin, Lang'fang, Baoding, Tangshan, and Cangzhou are shown in Fig. S3. Five HEs were identified in Tianjin with the revised criteria: 1 to 4 January, 15 to 19 January, 21 to 23 January, 25 to 29 January, and 7 to 14, February 2020. The statistics for each HE in each city are given in Table S1. Among the five HEs in the six cities, HE3 was the shortest episode (2–3 days) while HE5 was the longest (5–8 days). The severest pollution was observed in Baoding with a recorded maximum hourly $PM_{2.5}$ concentration exceeding 570 μg m^{-3} during HE4, followed by 373 μg m^{-3} in HE2 also observed in Baoding. Tianjin is also a pollution hotspot during the five HEs, with a maximum hourly $PM_{2.5}$ concentrations during each HE ranged from 199 to 293 μg m^{-3}. The maximum spatial scales covered by the five HEs were roughly assessed and shown in Fig. S4. The five HEs covered over half of the NCP. In terms of the recorded maximum spatial scales, the three HEs occurring before the COVID-19 outbreak covered a relatively larger area than the later two HEs appeared during the shutdown period.

3.2. Different meteorological features of the haze episodes

The time series of the surface $PM_{2.5}$ and meteorological parameters over the whole campaign are shown in Fig. 1. The hourly ventilation coefficients (VC, a measure of local dispersion conditions, defined as the product of wind speed and MLH) during the five HEs are shown in Fig. 2a and the boxplots of the meteorological parameters during each HE are available in Fig. S5. Calculations of the hourly air mass backward trajectories arrived at 100 m AGL are provided in Text S2. Detailed evolution of each HE is presented in Text S3.

HE1 was due to poor local dispersion with less regional transport given weak chemical reactivity. During the accumulation stage of HE1, the average VC is 300.7 m^2 s^{-1}, with minimum hourly VC being 7.2 m^2 s^{-1}. The average air mass speed in this interval was only 2.1 m s^{-1} (the average length of 48 h air mass backward trajectories was 368 km, Fig. 2b), which is the smallest compared to the other HEs. The slow motion of the air mass indicated that regional transport was weak and covered only a limited region. Measurements from the ground-based aerosol lidar suggested that the aerosol layer during HE1 appears to be the shallowest amongst the five HEs (Fig. 3), again indicating the poor dispersion and more local nature of the pollution sources. Both RH and radiation during HE1 were the lowest among the five HEs (Fig. S5), with hourly values almost always below 80% and 600 W m^{-2}, respectively. Thus, HE1 was likely formed under such surface meteorology that favorable for the physical accumulation rather than chemical formation

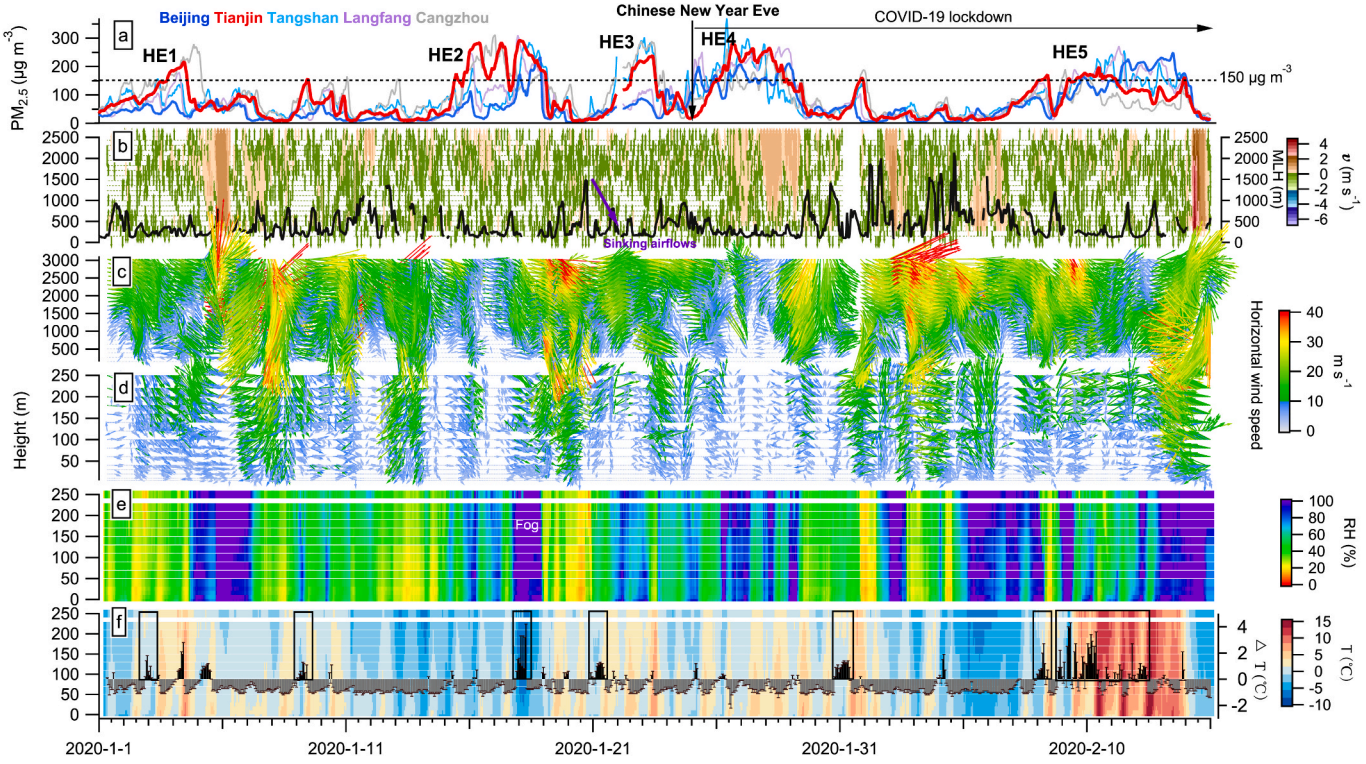

Fig. 1. Time series of $PM_{2.5}$ measured in Beijing, Tianjin, Tangshan, Lang'fang and Cangzhou (a), MLH and vertical winds within 2500 m AGL (b), horizontal winds measured via wind profiler radar (c) and meteorological tower (d), relative humidity (e) and air temperature recorded at meteorological tower, and temperature inversion between 250 m and 110 m AGL (f). The black rectangles in subplot of (f) denote the periods of inversion.

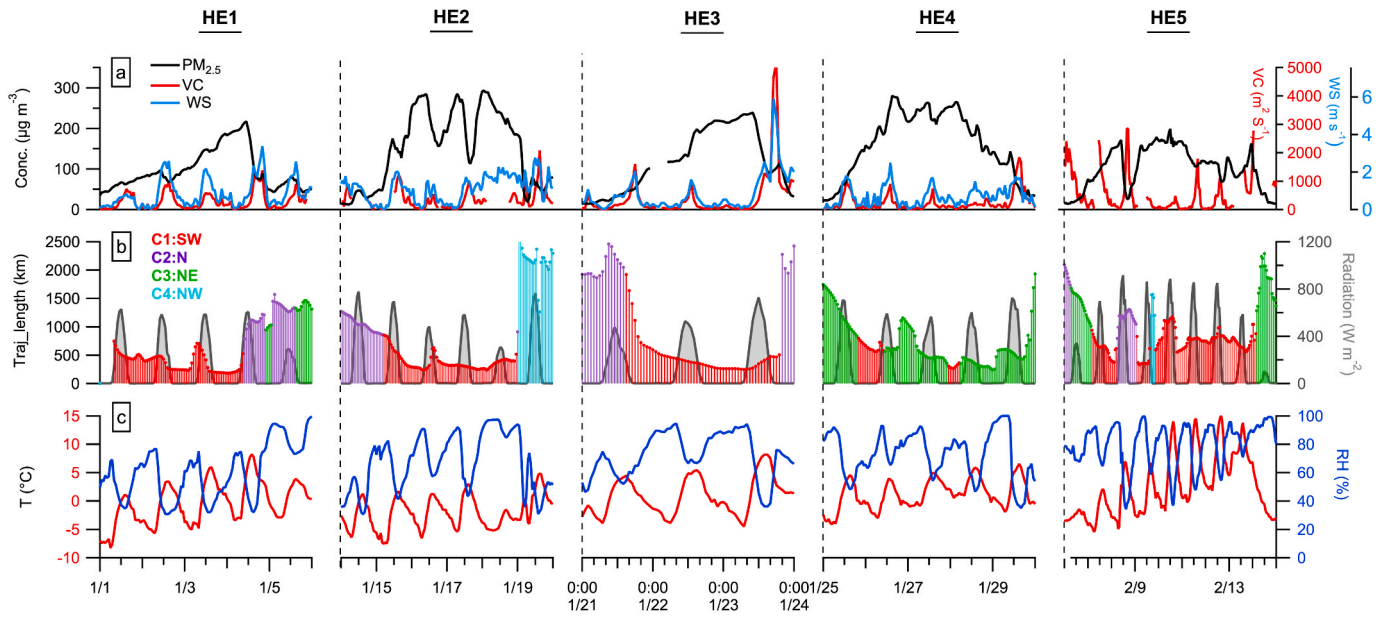

Fig. 2. Time series of averaged $PM_{2.5}$, VC and WS in Tianjin (a), radiation and the length of 48-h air mass backward trajectory (b), surface temperature and relative humidity (c) for the five HEs observed at NKU supersite. The hourly air mass trajectories were colored with their corresponding clusters (Fig. S6, cluster 1: SW, cluster 2: N, cluster 3: NE, and cluster 4: NW).

of PM.

HE2 featured intensive near-surface transport, strong inversions. The interquartile range (IQR) of both VC and MLH values during HE2 were lower than that during HE1 (Fig. S5). However, the surface wind speed was higher than that during HE1. From the aerosol lidar measurement (Fig. 3), it was unlikely that downmixing transport occurred during the accumulated stage of both HE1 and HE2. However, near-surface transport was relatively important compared to downmixing. This effects can be seen in the final $PM_{2.5}$ peak during HE2 that appears in Tianjin ahead of those in Lang'fang, Beijing and Tangshan (Fig. 1a), suggesting pollution transport from south to north in the BTH region. Therefore, local pollutants were heavily mixed with near-surface transported PM originating from upwind polluted areas (southwesterly). Concentrations were enhanced by a persistent strong temperature inversion above the fog (>200 m AGL) over night on 17 January (Fig. 1e&f), leading to the highest hourly rate of increase among the five HEs (~48 μg m^{-3} $PM_{2.5}$ per hour).

HE3 had stagnant surface weather coupled with persistent downmxing from above. HE3 was also related to the poor local dispersion with an average VC of 254 m^2 s^{-1}, and was enhanced by strong and persistent downmixing of PM from southwest of the region. Before $PM_{2.5}$ attained its maximum value, the MLHs remained below 500 m, surface wind speeds were less than 1.0 m s^{-1}, and the average air masses speed was approximately 1.5 m s^{-1}. In this stagnant environment, the surface temperature was below 0 °C and RH was approximately 90%. $PM_{2.5}$ gradually increased from the afternoon of 22 January to the next morning when it attained its maximum value (239 μg m^{-3}), accompanied by strong sinking of PM from >1.0 km AGL down to the ground. Measurement from the wind profiler radar also showed strong downward winds (Fig. 1b) associated with the decending aerosol layer (Fig. 3) that was transported from southwest (Fig. 2b).

HE4 formed gradually after midnight of 24 January (Chinese New Year Eve) when the direction of the transported air masses shifted from N-NE to SW (Fig. 2b). The fireworks tracer species (SO_2, Cl^-, K^+ and Mg^{2+}) and CO concurrently rose with $PM_{2.5}$ (Fig. 4). These results suggest that the increased $PM_{2.5}$ may be primarily from fireworks emissions. Note that fireworks displays were banned throughout Tianjin, but bans were not in place for other cities in the BTH areas, particularly in the rural areas where fireworks were extensively used. Before $PM_{2.5}$ reached its peak value, the air mass transport shifted from SW to NE with average speed of ~3.0–4.0 m s^{-1} (Fig. 2b), and the northeasterly surface wind speed increased. Thus, the fireworks emissions were able to be transported from the rural areas surrounding Tianjin. Among the five HEs, HE4 was characterized by VC values with the narrowest interquartile range (IQR) and the lowest average value (201 m^2 s^{-1}) (Fig. S5). The air mass trajectories for HE1, HE2, HE3, and HE5 largely originated from the southwest, while HE4 was heavily affected by northeasterly transported pollutants (Fig. 2b). This transport would have brought additional coal/biomass burning emissions from a tradition of "Sheng Wang Huo" in northern China in which a large pillar of coal and wood is set alight, generally on New Year's eve and burns for up to 5 days.

HE5 began just before the start of the Lantern Festival (February 8, 2020) and was accompanied by persistent inversions formed through repeated downmixing events. HE5 had the widest IQR of VC values and air mass trajectory lengths. The average VC for HE5 was 423 m^2 s^{-1}, which was the highest level among the five HEs. The last two HEs occurred during the COVID-19 shutdown and have longer trajectories (Fig. S5). Thus, there was faster transport speeds than during the first three HEs. Therefore, regional transport was much stronger during the last two HEs.

All five HEs in Tianjin featured poor local dispersion meteorology and involved near-surface transport with likely source regions primarily located to the southwest and northeast areas of the BTH region. In terms of local dispersion conditions for the five HEs, HE5 appeared to be associated with more favorable dispersion (higher VCs) while the other HEs had unfavorable dispersion conditions with HE4 having the lowest dispersion conditions. The measured CO was strongly correlated with $PM_{2.5}$ during the five HEs, particularly for the HE1 and HE2 with squared correlation coefficients of 0.87 and 0.86, respectively, suggesting substantial local sources. The sinking regionally transported aerosol also affected the fluctuations of $PM_{2.5}$ during both HE4 and HE5 as suggested by the significant decreases of the aerosol layer with downward winds observed simultaneously with increased $PM_{2.5}$ in the last two HEs. HE1 was the least affected by regional transport among the five HEs. The observed RH values during HE2-HE5 were much higher than that during HE1 (Fig. S5). The higher RH was favorable to enhanced aqueous-phase and/or heterogeneous chemistry (Cheng et al.,

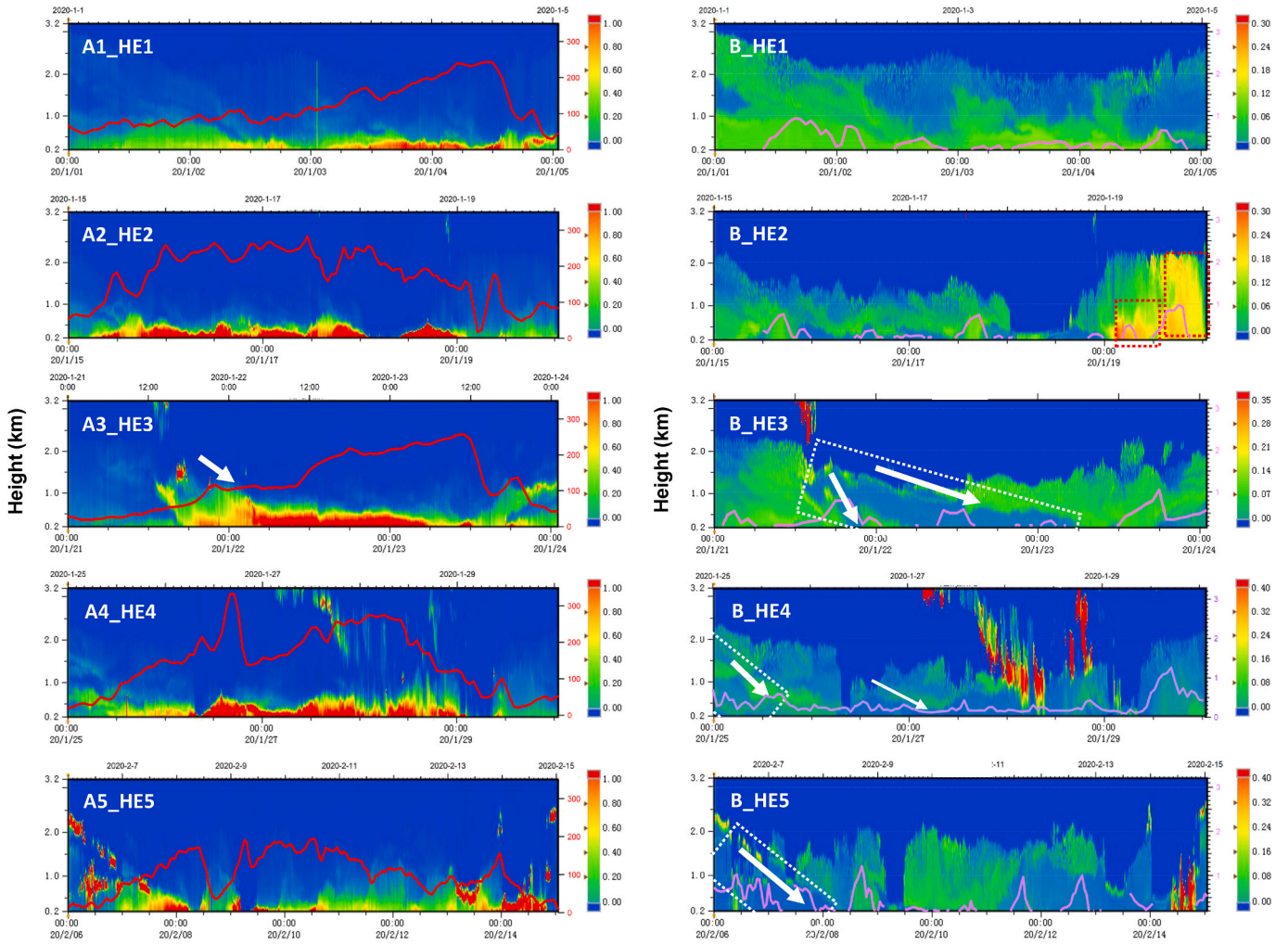

Fig. 3. Time series of the vertical profiles of aerosol extinction coefficients (left panel) and the vertical profiles of aerosol depolarization ratios (right panel) measured with an aerosol lidar at NKU supersite. Red lines and purple lines are the $PM_{2.5}$ concentrations and the MLH measured with ceilometer, respectively. (For interpretation of the references to color in this figure legend, the reader is referred to the Web version of this article.)

2016; Wang et al., 2016). As a further indication of the condensation of water on the individual particles and the resulting change in particle shape, the accumulation stages of $PM_{2.5}$ in all events but HE1 were accompanied by low depolarization ratio (Fig. 3), this result could be partially explained by the fact that the number of non-spherical particles (e.g., dust) tends to decrease through hygroscopic swelling under high RH environments, or the increased formation of secondary particles. Additionally, O_3 increased during the shutdown period (Fig. S3) that was due in part to increased solar insolation and higher temperatures but also the decrease in NO_x emissions from the lower level of vehicular use.

3.3. *Contributing sources of $PM_{2.5}$ during the haze episodes*

Concentrations and mass fractions of the measured $PM_{2.5}$ chemical species as well as source contributions are shown in Fig. 4. The average $PM_{2.5}$ source contributions during each HE are shown in Fig. S7. The $PM_{2.5}$ during HE1 largely originated from primary emissions in which coal combustion emissions contributed more than half of $PM_{2.5}$ mass (63.7%) followed by traffic emissions (10.2%). Both SO_2 and NO_2 significantly correlated with $PM_{2.5}$ during HE1, with squared correlation coefficients of 0.68 and 0.77 (Table S2), respectively. Heating demand increased during January due to the higher heating degree days in January (Fig. S8). Thus, the pollutant concentrations during HE1 were raised by emissions from fossil fuel combustion that accumulated under the poor dispersion conditions as described in Section 3.2. The variations of gaseous pollutants during HE2 were poorly correlated with each other compared to HE1 (Table S2). The SO_2 concentrations were lower in HE2 than in HE1, while NO_2 values were higher than in HE1 (Fig. S3). $PM_{2.5}$ was strongly correlated with CO ($r^2 = 0.87$). This result suggests that vehicle emissions were likely higher in importance in HE2 compared to HE1. $PM_{2.5}$ was poorly correlated with SO_2 during the other HEs. SIA was the predominant components of $PM_{2.5}$ during both HE2 and HE3, with average mass fractions of 73.0% and 71.2%, respectively, suggesting transported aerosol. In HE4, emissions from fireworks and residential burning was almost the exclusive $PM_{2.5}$ source during the first peak with an average mass fraction of >80%. In HE4 after 27 January, the contribution of fireworks and residential burning declined while SIA rose. SIA was also the dominant component of $PM_{2.5}$ during HE5 (50.1%). Since HE5 appeared at the beginning of Lantern Festival, the variation of $PM_{2.5}$ was also affected by fireworks and residential burning emissions (33%), particularly during the peak periods. Note that residential coal buring was also likely an additional source of ambient sulfate, which was one of the major component of $PM_{2.5}$ particularly in the later four HEs. As shown in Fig. S9, there was a clear upper edge in the scatter plot of sulfate with EC, demonstrating that those particles with high sulfate per unit EC probably emitted from coal burning as they are relatively high in arsenic (Dai et al., 2019).

During the two pandemic HEs during shutdown, traffic emissions contributed 1.7% and 1.8% of $PM_{2.5}$ mass on average, respectively. Dust

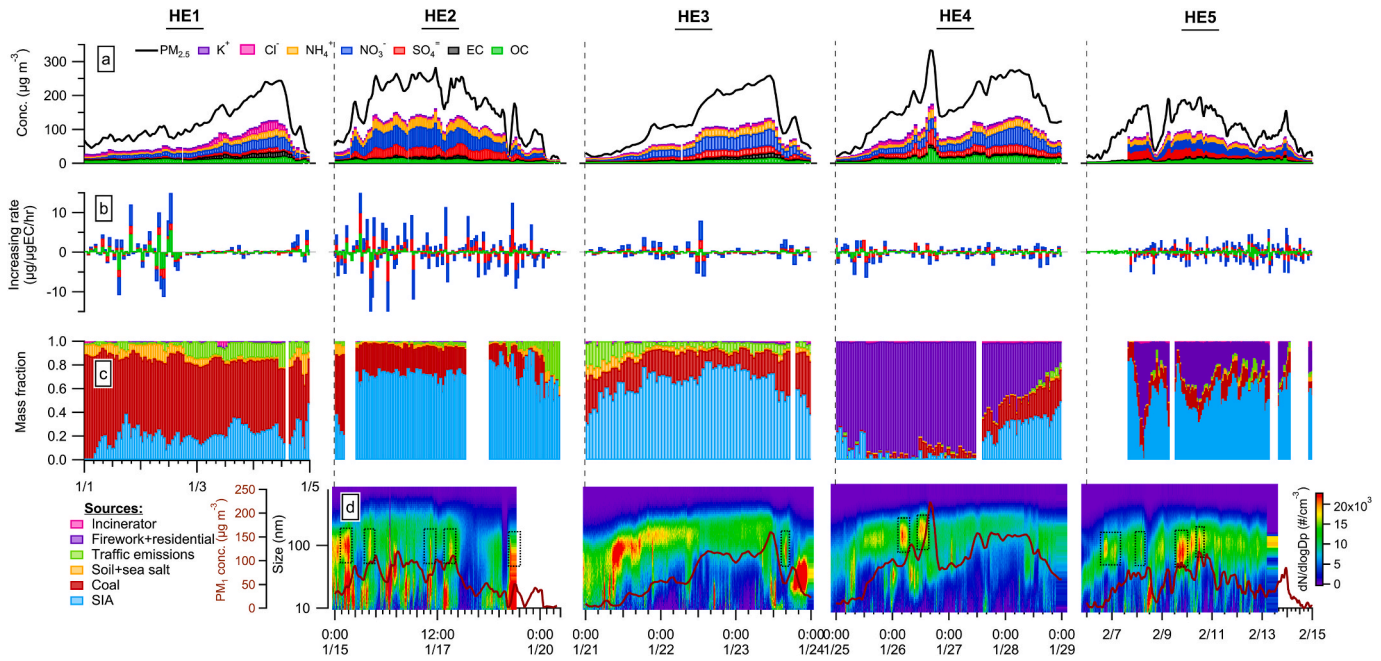

Fig. 4. Time series of mass concentrations of $PM_{2.5}$ and its chemical species (a), increasing rates of SO_4^{2-}/EC, NO_3^-/EC and OC/EC (b), mass fraction of sources in $PM_{2.5}$ (c), and PM_1 concentrations and size distribution of particle number concentrations (d) for the five observed HEs. The black dash rectangles in subplot (**d**) indicate the periods with potential regional transport. Note that the $PM_{2.5}$ was measured at NKU supersite.

(soil) + aged sea salt decreased to its lowest level (~1%) compared to the first three HEs. Reduced traffic volume would result in decrease suspension of road dust. Support for this attribution was provided by the aerosol lidar measurements that showed that the aerosol layers of HE1 and HE3 had larger depolarization ratios than other HEs since dust was mixed with more spherical particles (Fig. 3). The dramatic decline of traffic emissions and soil after the shutdown began demonstrates the positive responses to shutdown measures on air quality. Given that home quarantine and social distancing measures were in place during the lockdown, the time people spent at home was extended, leading to increased energy demand for heating/cooking. More residential coal/biomass would be expected to be consumed in suburban/rural residential areas (Shen et al., 2020). The extensive fireworks displays also occurred there during both the Spring Festival and Lantern Festival periods. Given that NO_x emitted from vehicles substantially decreased with the reduced traffic volume, secondary nitrate formed via the oxidation of NO_x was primarily attributed to coal combustion (coal-fired power plant, district heating, and residential coal burning) after the shutdown began (Dai et al., 2020). Therefore, the various coal combustion processes were likely the predominant sources of $PM_{2.5}$ during the shutdown with various particulate species augmented by the fireworks emissions.

4. Conclusions

The BTH area suffered severe HEs at the beginning of 2020, even after the COVID-19 shutdown measures were put into effect. This work investigated the formation of five HEs occurred before and during the shutdown by analyzing a comprehensive dataset mainly collected in Tianjin. The maximum hourly $PM_{2.5}$ concentrations of the five HE in Tianjin ranged from 199 to 293 μg m^{-3} and lasted from 2 days to over 1 week, with the longest episode during the Spring Festival that coincided with the start of the shutdown. Three HEs recorded before the shutdown began were related to accumulated primary pollutants and enhanced secondary aerosol under unfavorable dispersion conditions. Strong temperature inversions were occasionally appeared further exacerbating the pollution, resulting in an extremely high rate of increase of 48 μg m^{-3} $PM_{2.5}$ per hour during the second HE.

We found that the common "business as usual" emissions from local primary sources in this highly polluted area already exceeded the wintertime atmospheric diffusive capacity, since intensive haze formed under these adverse meteorological conditions. For example, in the first HEs. SIA was the predominant source of $PM_{2.5}$ during both HE2 and HE3 (>70%), consistent with existing literature reports. Positive air quality responses to the shutdown measures were found in the reductions in traffic emissions and dust (soil) + aged sea salt during the last two HEs that coincided with the Spring and Lantern Festivals, respectively. Holiday activites contributed large quantities of pollutants that highly affected the surrounding areas and exacerbated the air pollution. $PM_{2.5}$ sources during the beginning of both HE4 and HE5 were almost exclusively fireworks and residential burning. Emission reductions from the shutdown measures were insufficient to prevent the occurrence of HEs. Although the government has begun a program of replacing solid fueled residential stoves with natural gas, liquid petroleum gas, or electrical appliances, it is clearly necessary to complete this program to eleminate residential burning emissions as quickly as possible to provide the cleaner air that was to be the result of the stringent control measures imposed on other sources.

Credit author statement

Qili Dai: Writing- Original draft preparation. Jing Ding: Data curation, Writing - Review & Editing. Linlu Hou: Result interpretation. Linxuan Li: Data visualization. Ziying Cai: Meteorological data collection. Baoshuang Liu: Resources, Data collection. Congbo Song: Writing - Review & Editing. Xiaohui Bi: Resources, Data collection. Jianhui Wu: Sample collection and analysis. Yufen Zhang: Writing - Review & Editing. Yinchang Feng: Resources, Supervision and leadership. Philip K Hopke: Results interpretation, Writing - Review & Editing.

Declaration of competing interest

The authors declare that they have no known competing financial interests or personal relationships that could have appeared to influence

the work reported in this paper.

Acknowledgments and Data

This work was financially supported by the National Key R&D Program of China (grant no. 2016YFC0208505) and Tianjin Science and Technology Program (grant no. 18ZXSZSF00160). The authors thank Dr. Zhimei Xiao from Tianjin Eco-Environmental Monitoring Station for providing the measured MLH data.

Appendix A. Supplementary data

Supplementary data to this article can be found online at https://doi.org/10.1016/j.envpol.2021.117252.

References

Chang, X., Wang, S., Zhao, B., Cai, S., Hao, J., 2018. Assessment of inter-city transport of particulate matter in the Beijing-Tianjin-Hebei region. Atmos. Chem. Phys. 18 (7), 4843–4858. https://dio.org/10.5194/acp-18-4843-2018.

Chang, X., Wang, S., Zhao, B., et al., 2019. Contributions of inter-city and regional transport to PM2.5 concentrations in the Beijing-Tianjin-Hebei region and its implications on regional joint air pollution control. Sci. Total Environ. 660, 1191–1200. https://dio.org/10.1016/j.scitotenv.2018.12.474.

Chang, Y., Huang, R., Ge, X., et al., 2020. Puzzling haze events in China during the coronavirus (COVID-19) shutdown. Geophys. Res. Lett. 47 (12). https://dio.org/ARTN10.1029/2020GL088533.

Cheng, Y., Zheng, G., Wei, C., et al., 2016. Reactive nitrogen chemistry in aerosol water as a source of sulfate during haze events in China. Sci Adv 2 (12). http://advances.sciencemag.org/cgi/content/full/2/12/e1601530/DC1.

Dai, Q., Bi, X., Song, W., et al., 2019. Residential coal combustion as a source of primary sulfate in Xi'an, China. Atmos. Environ. 196, 66–76. https://doi.org/10.1016/j.atmosenv.2018.10.002.

Dai, Qili, Ding, Jing, Song, Congbo, Liu, Baoshuang, Bi, Xiaohui, Wu, Jianhui, Zhang, Yufen, Feng, Yinchang, Hopke, Philip, 2020a. Changes in source contributions to particle number concentrations afterthe COVID-19 outbreak: Insights from a dispersion normalized PMF. Sci. Total Environ. 759 https://doi.org/10.1016/j.scitotenv.2020.143548.

Dai, Q.L., Liu, B.S., Bi, X.H., et al., 2020b. Dispersion normalized PMF provides insights into the significant changes in source contributions to PM2.5 after the COVID-19 outbreak. Environ. Sci. Technol. 54 (16), 9917–9927. https://dio.org/10.1021/acs.est.0c02776.

Geng, G.N., Xiao, Q.Y., Zheng, Y.X., et al., 2019. Impact of China's air pollution prevention and control action plan on PM2.5 chemical composition over eastern China. Sci. China Earth Sci. 62 (12), 1872–1884. https://dio.org/10.1007/s11430-018-9353-x.

Huang, X., Ding, A., Gao, J., et al., 2020. Enhanced secondary pollution offset reduction of primary emissions during COVID-19 lockdown in China. Natl Sci Rev 1–9. https://doi.org/10.1093/nsr/nwaa137, 0.

Lai, Y., Brimblecombe, P., 2020. Changes in air pollution and attitude to fireworks in Beijing. Atmos. Environ. 231.

Le, T.H., Wang, Y., Liu, L., et al., 2020. Unexpected air pollution with marked emission reductions during the COVID-19 outbreak in China. Science 369 (6504), 702. https://dio.org/10.1126/science.abb7431.

Lv, Z., Wang, X., Deng, F., et al., 2020. Source−Receptor relationship revealed by the halted traffic and aggravated haze in beijing during the COVID-19 lockdown. Environ. Sci. Technol. 54, 15660–15670. https://doi.org/10.1021/acs.est.0c04941.

Pang, N., Gao, J., Zhao, P., Wang, Y., Xu, Z., Chai, F., 2021. The impact of fireworks control on air quality in four Northern Chinese cities during the Spring Festival. Atmos. Environ. 244, 117958 https://doi.org/10.1016/j.atmosenv.2020.117958.

Shen, H., Shen, G., Chen, Y., et al., 2020. Increased Air Pollution Exposure Among the Chinese Population during the National Quarantine in 2020. https://doi.org/10.31223/osf.io/6d9rn.

Tian, Y.Z., Wang, J., Peng, X., Shi, G.L., Feng, Y.C., 2014. Estimation of the direct and indirect impacts of fireworks on the physicochemical characteristics of atmospheric PM10 and PM2.5. Atmos. Chem. Phys. 14 (18), 9469–9479.

Tian, Y., Zhang, Y., Liang, Y., et al., 2020. PM2.5 source apportionment during severe haze episodes in a Chinese megacity based on a 5-month period by using hourly species measurements: explore how to better conduct PMF during haze episodes. Atmos. Environ. 224. https://dio.org/ARTN10.1016/j.atmosenv.2020.117364.

Tiwari, S., Tunved, P., Hopke, P.K., et al., 2016. Observations of ambient trace gas and PM10 concentrations at Patna, Central Ganga Basin during 2013-2014: the influence of meteorological variables on atmospheric pollutants. Atmos. Res. 180, 138–149. https://dio.org/10.1016/j.atmosres.2016.05.017.

Vu, T.V., Shi, Z.B., Cheng, J., et al., 2019. Assessing the impact of clean air action on air quality trends in Beijing using a machine learning technique. Atmos. Chem. Phys. 19 (17), 11303–11314. https://dio.org/10.5194/acp-19-11303-2019.

Wang, H., Xu, J.Y., Zhang, M., et al., 2014a. A study of the meteorological causes of a prolonged and severe haze episode in January 2013 over central-eastern China. Atmos. Environ. 98, 146–157 https://dio.org/10.1016/j.atmosenv.2014.08.053.

Wang, H.C., Lu, K.D., Chen, X.R., et al., 2018. Fast particulate nitrate formation via N2O5 uptake aloft in winter in Beijing. Atmos. Chem. Phys. 18 (14), 10483–10495. https://doi.org/10.5194/acp-18-10483-2018.

Wang, L.T., Wei, Z., Yang, J., et al., 2014b. The 2013 severe haze over southern Hebei, China: model evaluation, source apportionment, and policy implications. Atmos. Chem. Phys. 14 (6), 3151–3173 https://dio.org/10.5194/acp-14-3151-2014.

Wang, Y., Yao, L., Wang, L., et al., 2014c. Mechanism for the formation of the January 2013 heavy haze pollution episode over central and eastern China. Sci. China Earth Sci. 57 (1), 14–25. https://dio.org/10.1007/s11430-013-4773-4.

Wang, Y., Li, W., Gao, W., et al., 2019. Trends in particulate matter and its chemical compositions in China from 2013-2017. Sci. China Earth Sci. 62 (12), 1857–1871. https://dio.org/10.1007/s11430-018-9373-1.

Xue, T., Liu, J., Zhang, Q., et al., 2019. Rapid improvement of PM2.5 pollution and associated health benefits in China during 2013-2017. Sci. China Earth Sci. 62 (12), 1847–1856. https://dio.org/10.1007/s11430-018-9348-2.

Zheng, G.J., Duan, F.K., Ma, Y.L., et al., 2016. Episode-based evolution pattern analysis of haze pollution: method development and results from Beijing, China. Environ. Sci. Technol. 50, 4632–4641.

Zhang, Q., Zhang, Y., Tong, D., et al., 2019. Drivers of improved PM2.5 air quality in China from 2013 to 2017. P Natl Acad Sci USA 116 (49), 24463–24469. https://dio.org/10.1073/pnas.1907956116.

Zhang, Z.Z., Wang, W.X., Cheng, M.M., et al., 2017. The contribution of residential coal combustion to PM2.5 pollution over China's Beijing-Tianjin-Hebei region in winter. Atmos. Environ. 159, 147–161. https://dio.org/10.1016/j.atmosenv.2017.03.054.

Zhu, N., Zhang, D., Wang, W., et al., 2020. A novel coronavirus from patients with pneumonia in China, 2019. N. Engl. J. Med. 382 (8), 727–733. https://dio.org/10.1056/NEJMoa2001017.